Applied Physics Letters ARTICLE pubs.aip.org/aip/apl

All-polymer organic solar cells with fused carbazole acceptors for indoor photovoltaics

Cite as: Appl. Phys. Lett. **127**, 123901 (2025); doi: 10.1063/5.0288001
Submitted: 28 June 2025 · Accepted: 30 August 2025 ·
Published Online: 22 September 2025

Yue Zhang, Bo Wang, Xin Li, Chengyi Xiao,[a] and Weiwei Li[a]

AFFILIATIONS

Beijing Advanced Innovation Center for Soft Matter Science and Engineering & State Key Laboratory of Organic-Inorganic Composites, Beijing University of Chemical Technology, Beijing 100029, People's Republic of China

Note: This paper is part of the Special Topic, High-Performance Thin-Film Indoor Photovoltaics.
[a]**Authors to whom correspondence should be addressed:** xiaocy@mail.buct.edu.cn and liweiwei@iccas.ac.cn

ABSTRACT

The rapid expansion of the Internet of Things (IoT) necessitates maintenance-free, high-efficiency power sources. Organic solar cells (OSCs), offering superior spectral alignment with indoor lighting, are promising candidates for indoor energy harvesting. Here, we develop a fused carbazole-based polymer acceptor (designated as PCzT) with a tailored optical bandgap, rigid planar backbone, and enhanced electron-transporting properties. As a result, devices incorporating this acceptor achieve a power conversion efficiency of 8.15% under AM1.5G illumination and 11.63% under 3000 K, 1000 lux indoor lighting—outperforming state-of-the-art polymer acceptors in indoor applications. Crucially, we correlate nanoscale morphology (e.g., phase purity and domain size) with device performance, revealing that optimized interfacial packing enhances charge extraction and suppresses recombination. These findings provide a direct guideline for designing stable, high-performance polymer acceptors toward efficient indoor OSCs.

The rapid expansion of the Internet of Things (IoT) has intensified the demand for sustainable and efficient energy solutions to power ubiquitous connected devices. Conventional power sources such as lithium-ion and coin-cell batteries, while widely adopted, require frequent replacement and contribute to environmental pollution through improper disposal. In this context, organic solar cells (OSCs) have emerged as promising alternatives due to their flexibility, lightweight design, transparency, and exceptional performance under low-light conditions.[1–6] Recent advances in non-fullerene acceptors (NFAs) and polymerized small-molecule acceptors (PSMAs) have propelled the power conversion efficiency (PCE) of OSCs beyond 20% and 19%, respectively.[7–10] Nevertheless, OSCs still lag behind competing technologies like perovskite solar cells (PSCs) in terms of both PCE and operational stability under standard AM1.5G illumination, hindering their commercial viability.[11] Notably, OSCs exhibit superior compatibility with indoor light spectra, where their absorption characteristics align more closely with the emission profiles of artificial light sources [e.g., light-emitting diodes (LED)], suggesting bright prospects for IoT applications.[12]

Indoor light spectra differ markedly from standard AM1.5G solar radiation, exhibiting a narrower wavelength range (300–700 nm) and irradiance levels three orders of magnitude lower.[13,14] Consequently, optimal light harvesting under such conditions requires photoactive materials with bandgaps tuned to ~1.9 to 2.0 eV.[12] The OSCs are particularly well-suited for this application due to their tunable energy levels and efficient exciton generation under low illumination. While crystalline silicon (c-Si) solar cells outperform conventional OSCs (e.g., PTB7:$PC_{71}BM$) under AM1.5G illumination (13.49% vs 8.43% PCE),[15] the scenario reverses under indoor lighting. For instance, under LED illumination (890 lux), OSCs achieve a PCE of 11.63%, surpassing the 9.65% efficiency of c-Si devices.[15] Recent advances have further pushed indoor OSCs to record efficiencies exceeding 33%, underscoring their potential for low-energy applications.[16] Despite these successes, challenges remain, including limited precision in bandgap engineering and morphological instability under thermal or light stress.[17,18] The PSMAs have emerged as a promising strategy to enhance OSC stability,[19] yet its application in indoor organic photovoltaics (OPVs) remains largely unexplored.

Carbazole-based molecules, with their rigid conjugated backbones and versatile chemical tunability, have emerged as promising materials for indoor photovoltaic applications.[20–23] Here, we report the synthesis of a carbazole-derived polymer acceptor, PCzT (Fig. 1), and systematically evaluate its performance under indoor illumination. The design incorporates long alkyl side chains to enhance solubility while maintaining a halogen-free structure with a wide bandgap

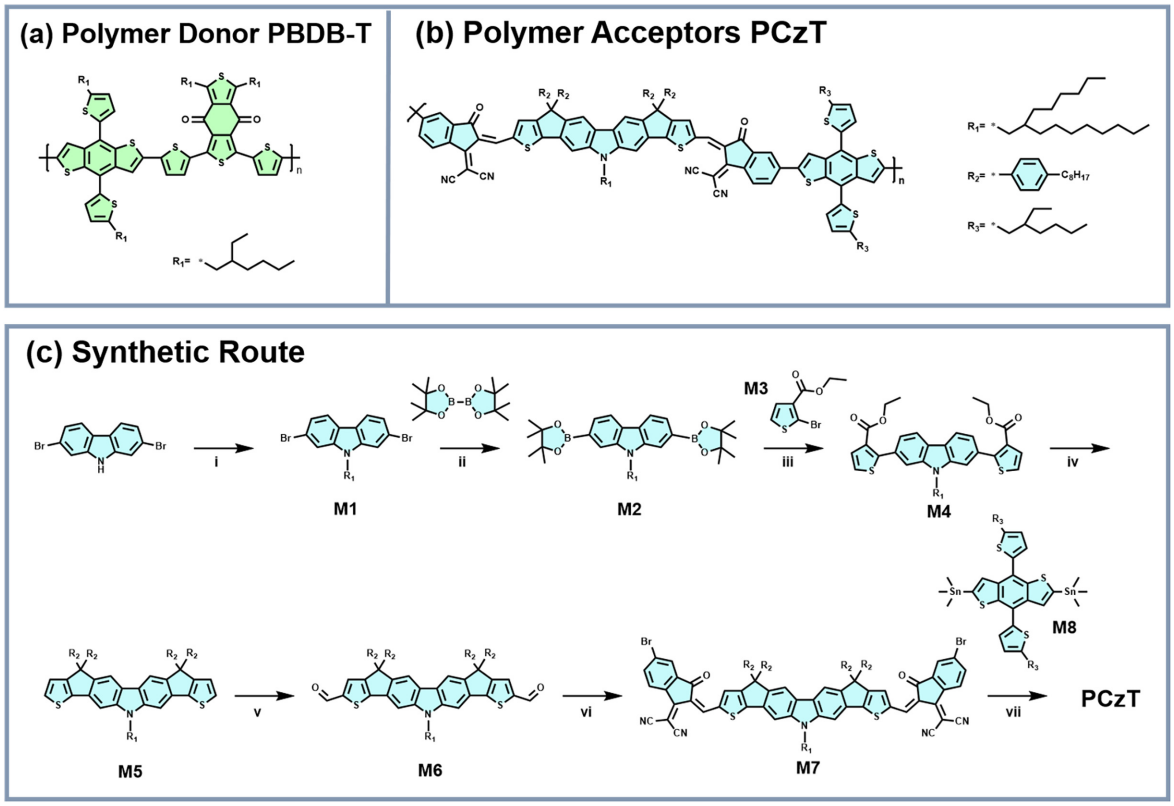

FIG. 1. Molecular structures of (a) the polymer donor and (b) the PSMA employed in this study. (c) Schematic representation of the synthetic pathway for polymer acceptor PCzT.

(~2.0 eV), ensuring optimal spectral alignment with indoor light sources. When fabricated into all-polymer OSCs, PCzT achieves a PCE of 8.15% under AM1.5G illumination. Notably, under indoor conditions (3000 K, 1000 lux), the PCE rises significantly to 11.62%, demonstrating its suitability for low-light environments. This work presents an absorption-compatible all-polymer solar cell optimized for indoor applications, providing a viable design strategy for efficient and stable indoor photovoltaics.

The molecular structures of donor PBDB-T and developed PSMA material PCzT are depicted in Figs. 1(a) and 1(b), respectively. The PCzT was synthesized via a *Stille* coupling reaction between the monomers **M7** and **M8**. The key monomer **M7** with a fused-ring carbazole structure was synthesized from 2,7-dibromocarbazole through a series of reactions with *N*-alkylation, *Suzuki* coupling, *Pictet–Spengler*, *Vilsmeier–Haack*, *Knoevenagel* condensation reaction, etc., and the details of the synthesis steps are shown in Fig. 1(c). Structural characterization of **M7** was confirmed by comprehensive proton nuclear magnetic resonance (^{1}H NMR) spectroscopy and matrix-assisted laser desorption/ionization time-of-flight (MALDI-TOF) mass spectrometry (supplementary material, Figs. S4–S9). PCzT was subsequently synthesized through *Stille* copolymerization followed by standard purification protocols (see the supplementary material for detailed procedures).

The molecular weight of PCzT was determined by high-temperature gel permeation chromatography (GPC) in 1,2,4-trichlorobenzene at 150 °C. As shown in Fig. S1, the polymer exhibits a number-average molecular weight (M_n) of 103.1 kDa, a weight-average molecular weight (M_w) of 227.5 kDa, and a polydispersity index PDI of 2.21. Figure 2(a) presents the UV–vis absorption spectra of PCzT in *o*-dichlorobenzene (*o*-DCB) solution and thin-film states. The polymer acceptor demonstrates characteristic absorption spanning 600–780 nm, while the donor exhibits dominant absorption between 400 and 600 nm. Notably, the absorption onset (λ_{onset}) of PCzT shifts only marginally from 728 nm (solution) to 722 nm (film), accompanied by slight spectral broadening, yielding an optical bandgap (E_g) of 1.58 eV. This minimal bathochromic shift suggests pre-aggregated states in solution, consistent with previous reports on similar conjugated polymers.[24]

The electrochemical properties of PCzT were characterized *via* cyclic voltammetry (CV, Fig. S2) to determine its energy levels [Fig. 2(b)]. The highest occupied molecular orbital (HOMO) and the lowest unoccupied molecular orbital (LUMO) energy levels are determined to be −5.59 and −3.90 eV, respectively. The large bandgap is advantageous for indoor OSCs, as it minimizes voltage losses under low-light illumination—a critical factor for high-efficiency indoor photovoltaics (Table I).

To evaluate its photovoltaic performance, the polymer acceptor PCzT was fabricated into the OSCs with the convert device configuration ITO/ZnO/PBDB-T:PCzT/MoO_3/Ag, where PBDB-T was selected as the donor because of its matching energy level. The *J–V* curve of the device under the AM1.5G illumination and the indoor light

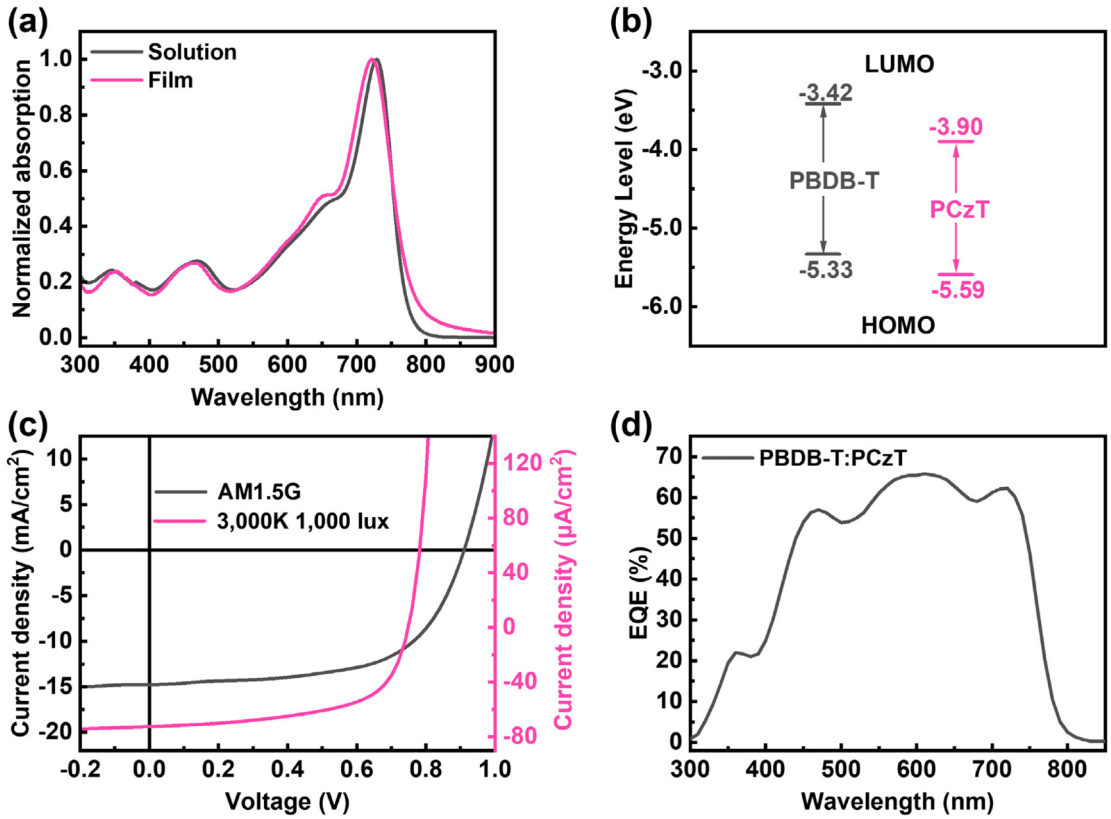

FIG. 2. (a) Normalized absorption spectra of PCzT in solution and thin film, respectively. (b) Energy level diagrams based on CV measurements for PBDB-T and PCzT. The (c) *J*–*V* and (d) EQE curves of all-polymer OSCs based on PBDB-T:PCzT blends.

TABLE I. Optical and electrochemical properties of PBDB-T and PCzT.

Polymers	λ_{onset}^{sol}[a] (nm)	λ_{onset}^{film}[b] (nm)	E_g^{film}[c] (eV)	E_{HOMO}[d] (eV)	E_{LUMO}[e] (eV)
PBDB-T	620	624	1.80	−5.33	−3.42
PCzT	728	721	1.58	−5.59	−3.90

[a]Absorption onset in *o*-DCB solution.
[b]Absorption onset in thin-film state.
[c]Optical bandgap was calculated through the onset of the thin-film absorption edge.
[d]Calculated by $E_{HOMO} = -4.80\,eV - E_{ox}$.
[e]$E_{LUMO} = -E_{red} - 4.80\,eV$.

(3000 K, 1000 lux) are both presented in Fig. 2(c). The corresponding LED emission spectra of 3000, 4000, and 5500 K are shown in Fig. S3. With a series of optimizations of processing conditions, the PCEs of the devices achieve a PCE of 8.15%, with an open-circuit voltage (V_{OC}) of 0.91 V, a short-circuit current density (J_{SC}) of 14.77 mA/cm^2, and a fill factor (FF) of 0.60. Under 3000 K, 1000 lux indoor LED light, the PCE increases to 11.62%, with a V_{OC} of 0.75 V, a J_{SC} of 72.48 μA/cm^2, and an FF of 0.60. The PCEs of this all-polymer OSC would slightly decrease to 10.14% and 8.97% for 4000 and 5500 K (1000 lux) indoor LED light, mainly owing to decreased J_{SC}s (Table II and Tables S1–S4). The higher V_{OC} under AM1.5G (0.91 V) illumination compared to indoor conditions (0.75 V) is primarily attributed to the reduced light intensity, which decreases the quasi-*Fermi* level splitting in the device. Notably, the V_{OC} of PBDB-T:PCzT-based OSCs remains high due to the acceptor's elevated LUMO level, which is beneficial for indoor applications where open-circuit voltage plays a critical role in efficiency. The J_{SC}s from *J*–*V* measurements closely match those derived from the external quantum efficiency (EQE) spectrum [Fig. 2(d) and Table II], with discrepancies within 5%, confirming reliable current extraction. This agreement further validates the device's charge collection efficiency under both illumination conditions.[12,25]

To investigate the charge transport ability of PCzT, we conducted the space-charge-limited-current (SCLC) measurement, as detailed in

TABLE II. Characteristics of all-polymer OSCs based on PBDB-T:PCzT under AM1.5G and indoor LED illumination, respectively.

Illumination	V_{OC}[a] (V)	J_{SC}[a,b]	J_{calc}[a,b,c]	FF[a]	PCE (%)
AM1.5G	0.91	14.77	14.08	0.60	8.15 (8.02 ± 0.13)
3000 K, 1000 lux	0.75	72.48	72.45	0.60	11.62 (11.42 ± 0.17)
4000 K, 1000 lux	0.75	66.10	65.48	0.58	10.14 (9.94 ± 0.19)
5500 K, 1000 lux	0.75	61.70	61.19	0.58	8.97 (8.78 ± 0.12)

[a]The average parameters are obtained from five devices.
[b]The units are mA/cm^2 for all-PSCs under AM1.5G illumination and μA/cm^2 for devices under indoor illumination.
[c]J_{calc} values are obtained by integrating the EQE spectra.

Fig. S2. The result revealed that the hole (μ_h) mobilities and the electron (μ_e) mobilities were 3.2×10^{-4} and 2.9×10^{-4} cm^2 V^{-1} s^{-1}, respectively. The μ_h/μ_e ratio was calculated to be 1.10, indicating balanced charge carrier mobilities, which facilitates more efficient charge transport channels within the devices and contributes to enhanced J_{SC} and FF of the OSCs.

Subsequently, to investigate the correlation between film morphology and photovoltaic performance of the OSCs, atomic force microscopy (AFM) and grazing-incidence wide-angle x-ray scatting (GIWAXS) measurement was conducted (Fig. 3). The AFM images reveal that the pristine PCzT film exhibits a mixed stacking morphology [Figs. 3(a) and 3(b)] with a low root mean square (RMS) roughness of 0.97 nm. In contrast, the PBDB-T:PCzT blend film displays distinct fibrous morphology [Figs. 3(c) and 3(d)] with a higher RMS roughness of 2.75 nm. This fibrous structure, characterized by interconnected nanoscale domains, is favorable for establishing continuous charge transport pathways between donor and acceptor phases, thereby enhancing exciton dissociation efficiency.

GIWAXS analysis further elucidates the molecular packing and orientation. Both pristine PCzT and PBDB-T:PCzT films exhibit a (010) π–π stacking peak in the out-of-plane (OOP) direction and a (100) alkyl chain packing peak in the in-plane (IP) direction. This indicates that the rigid conjugated backbone of PCzT predominantly adopts a face-on dominated orientation, which is preserved in the blend film.

The calculated coherence length (*CCL*) values of the (010) peak show no significant change between the pure and blend films, while the q value of the blend film slightly increases from 1.51 Å^{-1} for the as-cast film to 1.59 Å^{-1} for the blend film, indicating favorable compatibility between the donor and acceptor (Table S4). In contrast, the (100) peak in the IP direction shows identical q values of 0.27 Å^{-1} for these two films, while the *CCL* value (7.2 nm) of the blend is noticeably larger than 4.1 nm of the pure film, indicating that the donor induces a more ordered lamellar stacking within the blend film.

In conclusion, aiming at the energy supply challenges in IoT applications, we constructively proposed a strategy based on indoor organic photovoltaics. A carbazole-based polymer acceptor, PCzT was designed and synthesized with an absorption range well matched to the indoor light spectrum. When applied in indoor OSCs, PCzT, exhibited a PCE of 11.63% under 3000 K, 1000 lux illumination. Furthermore, we systematically investigated its optical properties, physical characteristics, and the phase separation behavior in the thin films, providing insight for the future development of high-performance indoor organic acceptor materials.

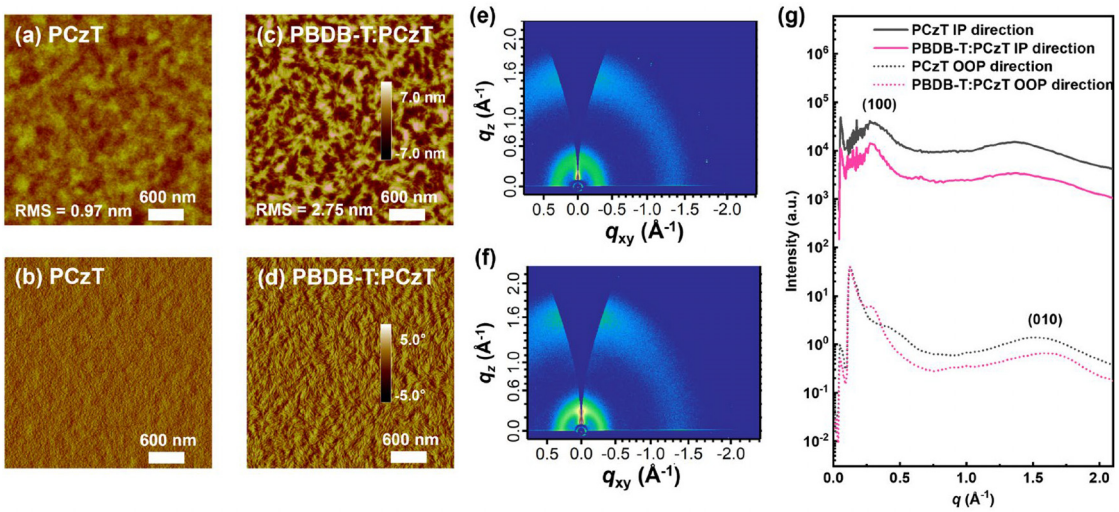

FIG. 3. AFM (a), (c) height and (b), (d) phase images of as-cast PCzT and PBDB-T:PCzT blended films, respectively. The RMS roughness is also included. The GIWAXS images of (e) as-cast PCzT and (f) PBDB-T:PCzT blends, respectively. (g) IP and OOP line-cuts of the corresponding GIWAXS images.

See the supplementary material for additional details on the materials and measurements, synthetic procedure, GPC and CV measurements, LED emission spectra and SCLC measurements, all-PSCs, GIWAXS/NMR/MS spectra, etc.

This study was jointly supported by the National Natural Science Foundation of China (52473165, 22475013) and the Fundamental Research Funds for the Central Universities of Beijing University of Chemical Technology (buctrc201828, XK1802-2).

AUTHOR DECLARATIONS

Conflict of Interest

The authors have no conflicts to disclose.

Author Contributions

Yue Zhang: Data curation (equal); Formal analysis (equal); Investigation (equal); Methodology (equal). **Bo Wang:** Data curation (equal); Formal analysis (equal); Investigation (equal); Methodology (equal); Writing – original draft (equal). **Xin Li:** Data curation (equal); Formal analysis (equal). **Chengyi Xiao:** Investigation (equal); Methodology (equal); Project administration (equal); Supervision (equal); Writing – review & editing (equal). **Weiwei Li:** Conceptualization (equal); Funding acquisition (equal); Methodology (equal); Supervision (equal); Writing – review & editing (equal).

DATA AVAILABILITY

The data that support the findings of this study are available within the article and its supplementary material.

REFERENCES

[1]C. Li, J. Zhou, J. Song, J. Xu, H. Zhang, X. Zhang, J. Guo, L. Zhu, D. Wei, G. Han, J. Min, Y. Zhang, Z. Xie, Y. Yi, H. Yan, F. Gao, F. Liu, and Y. Sun, Nat. Energy **6**, 605 (2021).
[2]Y. Cui, Y. Xu, H. Yao, P. Bi, L. Hong, J. Zhang, Y. Zu, T. Zhang, J. Qin, J. Ren, Z. Chen, C. He, X. Hao, Z. Wei, and J. Hou, Adv. Mater. **33**, 2102420 (2021).
[3]Q. Liu, Y. Jiang, K. Jin, J. Qin, J. Xu, W. Li, J. Xiong, J. Liu, Z. Xiao, K. Sun, S. Yang, X. Zhang, and L. Ding, Sci. Bull. **65**, 272 (2020).
[4]J. Yuan, Y. Zhang, L. Zhou, G. Zhang, H.-L. Yip, T.-K. Lau, X. Lu, C. Zhu, H. Peng, P. A. Johnson, M. Leclerc, Y. Cao, J. Ulanski, Y. Li, and Y. Zou, Joule **3**, 1140 (2019).
[5]M. J. Zhang, X. Guo, W. Ma, H. Ade, and J. H. Hou, Adv. Mater. **27**, 4655 (2015).
[6]B. Wang, J. N. Xu, Y. Lin, C. Y. Xiao, S. J. Liang, Z. Tang, C. R. Mcneill, and W. W. Li, Adv. Funct. Mater. **35**, 2418659 (2025).
[7]L. Chen, W. Liang, A. Sergeev, J. Y. L. Lai, X. Zeng, K. S. Wong, J. Zhang, S. H. Pun, H. Yan, and H. Hu, Energy Environ. Sci. **18**, 660 (2025).
[8]L. Liu, H. Li, J. Xie, Z. Yang, Y. Bai, M. Li, Z. Huang, K. Zhang, and F. Huang, Adv. Mater. **37**, 2500352 (2025).
[9]H. Li, J. Le, H. Tan, L. Hu, X. Li, K. Zhang, S. Zeng, Q. Liu, M. Zhang, L. Shi, Z. Cai, S. Liu, H. Li, L. Ye, X. Hu, and Y. Chen, Adv. Mater. **37**, 2411989 (2025).
[10]X. Wu, B. Xiao, R. Sun, X. Yang, M. Zhang, Y. Gao, B. Xiao, E. D. Papkovskaya, Y. Luponosov, C. J. Brabec, and J. Min, Energy Environ. Sci. **18**, 1812 (2025).
[11]Y. Cui, L. Hong, T. Zhang, H. Meng, H. Yan, F. Gao, and J. Hou, Joule **5**, 1016 (2021).
[12]H. S. Ryu, S. Y. Park, T. H. Lee, J. Y. Kim, and H. Y. Woo, Nanoscale **12**, 5792 (2020).
[13]B. Minnaert and P. Veelaert, Energies **7**, 1500 (2014).
[14]B. Minnaert and P. Veelaert, Adv. Sci. Technol. **74**, 170 (2010).
[15]S. Mori, T. Gotanda, Y. Nakano, M. Saito, K. Todori, and M. Hosoya, Jpn. J. Appl. Phys. **54**, 071602 (2015).
[16]W. X. Wang, Y. Cui, T. Zhang, P. Q. Bi, J. Q. Wang, S. W. Yang, J. W. Wang, S. Q. Zhang, and J. H. Hou, Joule **7**, 1067 (2023).
[17]X. Liu, S. Xu, B. Tang, and X. Song, Chem. Eng. J. **497**, 154944 (2024).
[18]S. Y. Park, C. Labanti, J. Luke, Y. C. Chin, and J. S. Kim, Adv. Energy Mater. **12**, 2103237 (2022).
[19]Z. G. Zhang and Y. F. Li, Angew. Chem., Int. Ed. **60**, 4422 (2021).
[20]C. Wei, Y. Yan, T. Zhang, Y. Zhao, and T. Yu, J. Mol. Struct. **1293**, 136312 (2023).
[21]Y.-J. Su, S.-C. Huang, T.-W. Chen, L.-C. Chueh, Y. Cui, L. Hong, H. F. Yao, J. H. Hou, J.-T. Chen, and C.-S. Hsu, ACS Appl. Mater. Interfaces **13**, 26247 (2021).
[22]L. Xie, Y. Zhang, W. Zhuang, S. Y. Jeong, Q. Bian, H. Li, J. Cao, W. Liu, H. Tan, H. Y. Woo, J. Zhang, and E. Wang, Chem. Eng. J. **427**, 131674 (2022).
[23]Suman, A. Siddiqui, M. L. Keshtov, G. D. Sharma, and S. P. Singh, J. Mater. Chem. C **7**, 543 (2019).
[24]B. M. Xie, K. Zhang, Z. C. Hu, H. Y. Fang, B. J. Lin, Q. W. Yin, B. T. He, S. Dong, L. Ying, and W. Ma, Sol. RRL **4**, 1900385 (2020).
[25]M. Mainville and M. Leclerc, ACS Energy Lett. **5**, 1186 (2020).